molecules

MDPI

Article

Polyaromatic *Bis*(indolyl)methane Derivatives with Antiproliferative and Antiparasitic Activity

Raquel C. R. Gonçalves [1,2], Pablo Peñalver [3], Susana P. G. Costa [1], Juan C. Morales [3] and Maria Manuela M. Raposo [1,*]

[1] Centre of Chemistry, University of Minho, Campus of Gualtar, 4710-057 Braga, Portugal; raquelrainha10@hotmail.com (R.C.R.G.); spc@quimica.uminho.pt (S.P.G.C.)
[2] Advanced (Magnetic) Theranostic Nanostructures Lab, International Iberian Nanotechnology Laboratory, Av. Mestre José Veiga s/n, 4715-330 Braga, Portugal
[3] Instituto de Parasitología y Biomedicina López Neyra, CSIC, PTS Granada, Avenida del Conocimiento 17, 18016 Armilla, Granada, Spain; pablo@ipb.csic.es (P.P.); jcmorales@ipb.csic.es (J.C.M.)
* Correspondence: author: mfox@quimica.uminho.pt

Abstract: *Bis*(indolyl)methanes (BIMs) are a class of compounds that have been recognized as an important core in the design of drugs with important pharmacological properties, such as promising anticancer and antiparasitic activities. Here, we explored the biological activity of the BIM core functionalized with different (hetero)aromatic moieties. We synthesized substituted BIM derivatives with triphenylamine, *N*,*N*-dimethyl-1-naphthylamine and 8-hydroxylquinolyl groups, studied their photophysical properties and evaluated their in vitro antiproliferative and antiparasitic activities. The triphenylamine BIM derivative **2a** displayed an IC_{50} of 3.21, 3.30 and 3.93 μM against *Trypanosoma brucei*, *Leishmania major* and HT-29 cancer cell line, respectively. The selectivity index demonstrated that compound **2a** was up to eight-fold more active against the parasites and HT-29 than against the healthy cell line MRC-5. Fluorescence microscopy studies with MRC-5 cells and *T. brucei* parasites incubated with derivative **2a** indicate that the compound seems to accumulate in the cell's mitochondria and in the parasite's nucleus. In conclusion, the BIM scaffold functionalized with the triphenylamine moiety proved to be the most promising antiparasitic and anticancer agent of this series.

Keywords: African trypanosomiasis; antiproliferative agent; antiprotozoal agent; *bis*(indolyl)methane derivatives; leishmaniasis

check for updates

Citation: Gonçalves, R.C.R.; Peñalver, P.; Costa, S.P.G.; Morales, J.C.; Raposo, M.M.M. Polyaromatic *Bis*(indolyl)methane Derivatives with Antiproliferative and Antiparasitic Activity. *Molecules* **2023**, *28*, 7728. https://doi.org/10.3390/molecules28237728

Academic Editor: Christoffer Bengtsson

Received: 15 October 2023
Revised: 17 November 2023
Accepted: 18 November 2023
Published: 23 November 2023

Copyright: © 2023 by the authors. Licensee MDPI, Basel, Switzerland. This article is an open access article distributed under the terms and conditions of the Creative Commons Attribution (CC BY) license (https://creativecommons.org/licenses/by/4.0/).

1. Introduction

Pathogenic protozoa are responsible for several diseases worldwide including human African trypanosomiasis (also known as sleeping sickness, caused by two subspecies of *Trypanosoma brucei*) and leishmaniasis (caused by more than 20 species of *Leishmania* spp.). Currently, these parasitic diseases do not have a FDA-approved vaccine [1–4], and the drugs used as treatments have many drawbacks such as toxicity, undesirable side effects, drug resistance, conditional efficiency (depending on the species causing the infection and the stage of disease) and high cost. In 2021, the US Food and Drug Administration (FDA) approved fexinidazole as the first all-oral treatment for both stages of the *Trypanosoma brucei gambiense* form of sleeping sickness [5]. Nevertheless, additional therapeutic options are needed for this parasitic infection, and especially for other tropical neglected diseases.

Bis(indolyl)methanes (BIM) are a class of heterocyclic compounds that have as their central core two indole units linked through a methylene group. This structure can be found as part of several natural products including arundine, vibrindole A, arsindoline A and arsindoline B (see Figure 1) [6–8]. BIM derivatives have been already shown to have interesting pharmacological activities such as anticancer [9–12], antibacterial [13,14], antioxidant [15,16], anti-inflammatory [17,18], antifungal [19] and antiviral agents [20], among

others. Indeed, the BIM core is recognized as an important scaffold and pharmacological intermediate in drug discovery; therefore, great effort has been devoted to the synthesis and chemical modification of *bis*(indolyl)methane and its analogues to gain further insight regarding the structure–activity relationship [21].

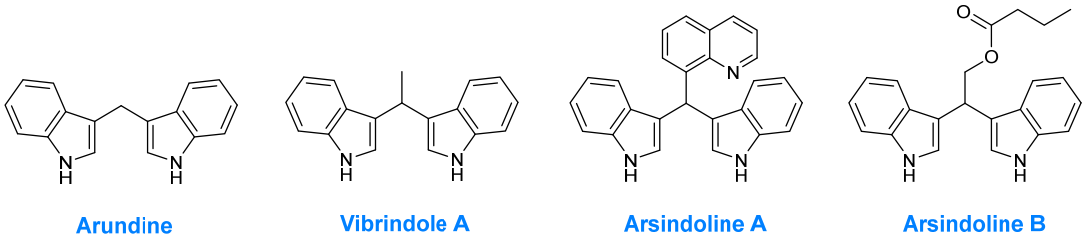


Figure 1. Structures of arundine, vibrindole A, arsindoline A and arsindoline B.

The antitumor activity and mechanism of action of *bis*(indolyl)methane and its derivatives have been widely investigated in several cancer cell lines [22–27]. However, to the best of our knowledge, research on the antiparasitic activity of this family of compounds has been scarce [28–32]. Most notably, Roy et al. reported that *bis*(indolyl)methane was active against *Leishmania donovani* (IC_{50} of 1.2 μM) through a mechanism of action that inhibits topoisomerase I and mitochondrial F0F1-ATP synthase [30,31]. Bharate et al. studied the antileishmanial, antimalarial, antibacterial and antifungal activities of different BIM derivatives. The structure–activity relationship analysis showed that *bis*(indolyl)methane functionalized with nitroaryl or heteroaromatic groups displayed promising antileishmanial activity (IC_{50} ranging from 3.02 to 15.94 μM), although the therapeutic window toward healthy cell lines was not reported [29]. Furthermore, the synergistic interaction of several *bis*(indolyl)methane-related indoles and other known antiparasitic drugs for the treatment and prevention of parasitic infections including malaria, leishmaniasis, trypanosomiasis, trichomoniasis, neosporosis and coccidiosis were protected under patent [33].

Drugs with dual anticancer and antiparasitic activities have been described in the literature. In fact, they possibly target related metabolic routes in tumor cells and parasites as well as other common therapeutic targets [34,35]. For example, carbohydrate naphthalene diimide conjugates (carb-NDIs) and stiff-stilbene derivatives have been reported as promising anticancer and antiparasitic agents whose mechanism of action is associated with high-affinity binding to nucleic G-quadruplex structures [36,37]. Moreover, other possible mechanisms of action of these dual drugs have been comprehensively reviewed and discussed by Zahra Dorosti et al. [34]. Yet, further research in this field is necessary.

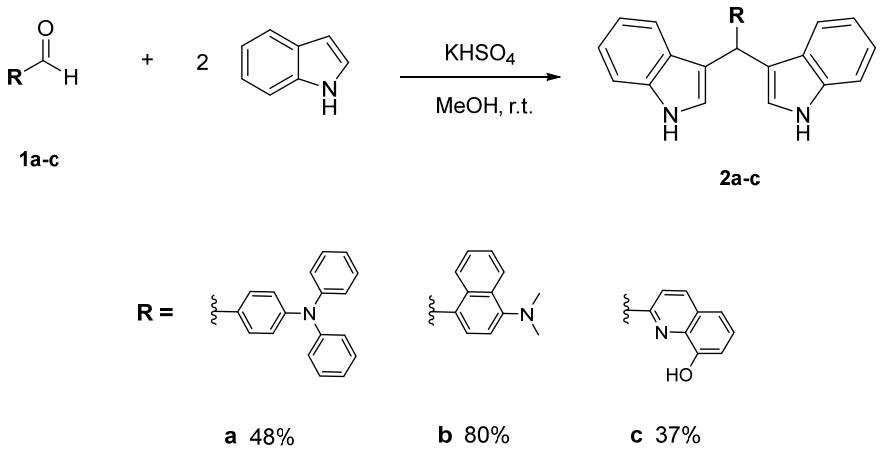
Having this in mind, our goal was to design, synthesize and evaluate the biological activity of a family of BIM derivatives **2a**–**c** functionalized with different hetero(aromatic) groups, including triphenylamine, *N*,*N*-dimethyl-1-naphthylamine and 8-hydroxylquinolyl. Here, we describe the synthesis of compounds **2a**–**c**, as well as the characterization of the structural and photophysical properties and evaluation of their biological activity as potential antiparasitic agents, specifically active against *T. brucei* and *L. major*. Additionally, due to the anticancer properties of previously reported BIM derivatives, the antiproliferative activity and selectivity of the synthesized compounds were also investigated in human cancer cell lines (endometrium and breast cancer cell lines) and compared to their activity in a healthy human cell line (fibroblasts).

2. Results and Discussion

2.1. Synthesis and Characterization of Bis(indolyl)methane Derivatives

A series of *bis*(indolyl)methane derivatives **2a**–**c** were synthesized, purified and characterized in order to evaluate phenotypically the influence of the different (hetero)aromatic moieties on in vitro biological models. As an overview, the route for the synthesis of the BIM derivatives substituted with triphenylamine, *N*,*N*-dimethyl-1-naphthylamine and 8-hydroxylquinolyl groups, is represented in Scheme 1, and the experimental data concern-

ing the synthesis and the structural and photophysical characterization of the compounds are shown in Table 1 and Figures S1–S6.



Scheme 1. Synthesis of *bis*(indolyl)methane derivatives **2a**–**c**.

Table 1. Synthesis and photophysical data in acetonitrile solution (absorption, λ_{abs}, and fluorescence emission maxima, λ_{fluo}, Stokes shift, Δ_{SS} and relative fluorescence quantum yields, ϕ_F) for the BIM derivatives **2a**–**c**.

Compound	Yield (%)	λ_{abs} (nm)	λ_{fluo} (nm)	Δ_{SS}(cm^{-1})	ϕ_F
2a	48	292	372	7365	0.28
2b	80	218	-	-	-
2c	37	241	483	20,790	0.01

The compounds were obtained in moderate to good yields (37–80%) through the condensation of indoles with the formyl precursors **1a**–**c** in dry methanol and in the presence of potassium hydrogen sulfate [38]. The synthesis of BIM derivative **2a** has been reported previously [39,40].

The photophysical properties of the *bis*(indolyl)methanes **2a**–**c** were investigated in acetonitrile solutions, and it was observed that the position of the absorption and emission bands were clearly dependent on the nature of the substituent group introduced in the *bis*(indolyl)methane core. Compound **2a** displayed the highest maximum absorption wavelength and the lowest maximum emission wavelength, resulting in a smaller Stokes shift (Δ_{SS} = 7365 cm^{-1}). Compound **2b** presented an absorption band at a lower wavelength (λ_{abs} = 218 nm), while compound **2c** exhibited the highest emission wavelength and the largest Stokes shift (Δ_{SS} = 20,790 cm^{-1}). Regarding the relative fluorescence quantum yields (ϕ_F), derivative **2a** showed modest fluorescence emission efficiency, whereas derivatives **2b**,**c** were much less fluorescent.

In fact, the position of the absorption bands were clearly dependent on the electronic nature of the substituent group: compound **2a** displayed the highest wavelength of maximum absorption, due to the extended intramolecular electron delocalization of the triphenylamine group as well as its electron-donating nature, and both compound **2b** and **2c**, bearing a naphthalene and quinoline moiety, respectively, showed blue-shifted absorption bands when compared to compound **2a**, probably due to their electron-deficient heterocyclic nature as well as the smaller size of the π-conjugated system.

2.2. Biological Phenotypic Activity

The biological activity of the *bis*(indolyl)methane derivatives **2a**–**c** were evaluated on in vitro models of parasites (*T. brucei* and *L. major*), human cancer cells (HeLa and HT-29) and human healthy cells (MRC-5). The toxicity of the BIM derivatives was determined through alamarBlue assay (for *T. brucei* and MRC-5) or MTT assay (for *L. major*), and the

results are expressed as the concentration of the compound that reduces cell viability by 50% calculated through dose-response curves to give half maximal inhibitory concentration (IC_{50}) (see Figures S7–S11).

To determine the therapeutic window, we calculated the selectivity index (SI) of each of the compounds. The SI is a ratio that measures the window between cytotoxicity in healthy cells and the antiparasitic/antiproliferative activity by dividing the cytotoxicity value (IC_{50} in MRC-5 cells) into the compounds' half maximal inhibitory concentration in parasites (IC_{50} in *T. brucei* and *L. major*) or cancer cells (IC_{50} in HeLa and HT-29). An SI value of 1 means that the compounds are as toxic for the healthy cell line as for the parasitic and cancer cell lines. When the SI value is bigger than 1, it means that the compounds are more active against the parasitic and cancer models than in the healthy cell line, with the magnitude of SI being the dimension of the therapeutic window. On the opposite side, an SI value lower than 1 means that the compounds are more toxic in the healthy cell line than against the parasites and cancer cells. The obtained results are presented in Table 2.

Table 2. Biological activity data for cytotoxicity in MRC-5, HeLa and HT-29 and antiparasitic activity against *T. brucei* and *L. major* represented as IC_{50} values (μM) with the error reported as σ. The selectivity index was calculated related to a healthy cell line (MRC-5).

Compound	IC_{50} μM					Selectivity Index (SI) *			
	T. brucei	*L. major*	MRC-5	HeLa	HT-29	*T. brucei*	*L. major*	HeLa	HT-29
2a	3.21 ± 0.04	3.30 ± 0.25	33.69 ± 3.19	37.53 ± 1.86	3.93 ± 0.49	10.50	10.21	0.90	8.57
2b	15.99 ± 4.44	>100	94.86 ± 7.27	89.56 ± 0.15	25.44 ± 5.23	5.93	<0.95	1.06	3.73
2c	14.66 ± 0.05	20.67 ± 1.71	3.25 ± 0.29	28.27 ± 5.01	71.36 ± 3.99	0.22	0.16	0.11	0.05

* SI = (IC_{50} MRC-5/IC_{50} parasite or cancer cell line).

Regarding the antiparasitic activity of the BIM family, prepared, derivative **2a**, substituted with the triphenylamine group, exhibited the highest activity of the series against both *T. brucei* and *L. major* with an IC_{50} of 3.21 μM and 3.30 μM, respectively. Interestingly, the cytotoxicity in normal human cells was found to be ten-fold lower (IC_{50} = 33.69 μM). Thus, compound **2a** presented an SI value of 10.50 and 10.21 for *T. brucei* and *L. major*, respectively, indicating an interesting therapeutic potential against both parasites. The unsubstituted analogue *bis*(indolyl)methane (arundine), previously reported as an inhibitor of topoisomerase I and mitochondrial F0F1-ATP synthase in *L. donavani* (species of Leishmania, also responsible for the disease leishmaniasis), displayed an IC_{50} of 1.2 μM, which is in the same range as compound **2a** in *L. major* [30,31].

Derivative **2b**, substituted with a *N*,*N*-dimethyl-1-naphthylamine group, showed a more modest inhibitory effect on *T. brucei* (with a IC_{50} = 15.99 μM) in comparison to compound **2a**, and very low toxicity in healthy MRC-5 cells as well as in *Leishmania major* parasites. As a result, for *T. brucei*, the SI value for **2b** was found to be 5.93, which was lower than that calculated for compound **2a**. Hence, the functionalization of the *bis*(indolyl)methane core with the *N*,*N*-dimethyl-1-naphthylamine group decreased the compound's activity in general, but most notably against *L. major* (IC_{50} > 100 μM), where the compound displayed no toxicity. In contrast to compounds **2a** and **2b**, compound **2c** displayed an IC_{50} of 14.66 and 20.67 μM in the *T. brucei* and *L. major* models, respectively, while being much more toxic towards the healthy MRC-5 cells (IC_{50} = 3.25 μM), resulting in an SI value lower than 1.

Due to the anticancer activity of different BIM derivatives previously reported [9–12], the activity of compounds **2a**–**c** against HeLa (human cervical carcinoma) and HT-29 (human colorectal adenocarcinoma) cell lines was also investigated. BIM derivatives **2a** and **2c** displayed IC_{50} values in the high micromolar range for HeLa cells, together with a poor selectivity index (0.90 and 0.11, respectively). On the other hand, the toxicity of compound **2a** against the HT-29 cell line was considerably higher compared to the HeLa cancer cell line ($IC_{50\ HT\text{-}29}$ = 3.93 μM vs. $IC_{50\ HeLa}$ = 37.53 μM) and showed an SI value of 8.57. Moreover,

this BIM derivative **2a** substituted with a triphenylamine group was significantly more toxic against HT-29 than its analogue arundine ($IC_{50\ HT\text{-}29}$ = > 100 μM) [41].

In silico models to predict ADMET (absorption, distribution, metabolism, excretion and toxicity) profiles are a valuable tool in medicinal chemistry research, enabling the identification of lead molecules with desired pharmaceutical properties. The ADMET lab2.0 online server [42] was used to predict relevant physicochemical, pharmacokinetic and toxicity endpoints of the synthesized BIM derivatives as well as arundine, a BIM natural product reported as an anticancer agent (Table 3). Overall, the analysis of the results revealed that all compounds satisfied Lipinski's rule of five (MW $\leq$ 500, LogP $\leq$ 5, nHA $\leq$ 10, nHD $\leq$ 5), which is a set of criteria used as guidelines to predict the likelihood of a compound being orally bioavailable and having favorable pharmacokinetic properties. Furthermore, the predicted toxicity results indicated that among the evaluated derivatives, compound **2a** displayed the safest drug profile, with low probability of both mutagenic and carcinogenic effects and rat acute oral toxicity.

Table 3. Physicochemical, pharmacokinetic and toxicity (ADMET) properties of the BIM derivatives, according to ADMET lab 2.0 software.

	Properties	Compound 2a	Compound 2b	Compound 2c	Arundine
Physicochemical	**MW**	489.22	415.2	389.15	246.12
	logP	7.363	6.249	5.281	4.185
	TPSA (Å^2)	34.82	34.82	64.7	31.58
	nHA	3	3	4	2
	nHD	2	2	3	2
	nRot	6	4	3	2
Medicinal chemistry	**Lipinski**	Accepted	Accepted	Accepted	Accepted
	PAINS	0 alerts	0 alerts	0 alerts	0 alerts
Absorption	**Caco-2 Permeability (log cm/s)**	−5.14 (Yes)	−5.14 (Yes)	−5.323 (No)	−4.852 (Yes)
	MDCK Permeability (cm/s)	4×10^{-6} (Yes)	7×10^{-6} (Yes)	5×10^{-6} (Yes)	9×10^{-6} (Yes)
Distribution	**VD (L/Kg)**	3.16 (Yes)	3.068 (Yes)	1.843 (Yes)	1.857 (Yes)
Metabolism	**CYP2C9 Substrate ***	0.94 (Yes)	0.96 (Yes)	0.96 (Yes)	0.97 (Yes)
Excretion	**CL (mL/min/kg)**	4.598	5.843	4.475	7.19

Table 3. *Cont.*

	Properties	Compound 2a	Compound 2b	Compound 2c	Arundine
Toxicity	**AMES Toxicity** *	0.053 (Low)	0.984 (High)	0.683 (Medium)	0.609 (Medium)
	Carcinogenicity *	0.159 (Low)	0.092 (Low)	0.053 (Low)	0.044 (Low)
	Rat Acute Oral Toxicity *	0.086(Low)	0.355 (Medium)	0.2 (Low)	0.202 (Low)

MW (molecular weight); LogP (predicted octanol/water partition coefficient): optimal 0–3; nHA (number of hydrogen acceptors): optimal 0–12; nHD (number of hydrogen donors): optimal 0–7; nRot (number of rotatable bonds): optimal 0–11; TPSA (topological polar surface area): optimal 0–140; Lipinski's rule: MW $\leq$ 500, LogP $\leq$ 5, nHA $\leq$ 10, nHD $\leq$ 5; PAINS (pan-assay interference compounds); Caco-2 permeability: optimal > -5.15; MDCK permeability (cm/s): optimal >2 $\times$ 10^{-6} cm/s; VD (volume distribution): optimal 0.04–20 L/kg; CL (clearance): >15 "high clearance", 5–15 "moderate clearance", <5 "low clearance". * Probability of being positive (0–1).

2.3. Fluorescence Microscopy of **2a**

The cellular uptake and localization of BIM derivative **2a** within MRC-5 cells and *T. brucei* parasites was studied using fluorescence microscopy, as shown in Figures 2 and 3, respectively.

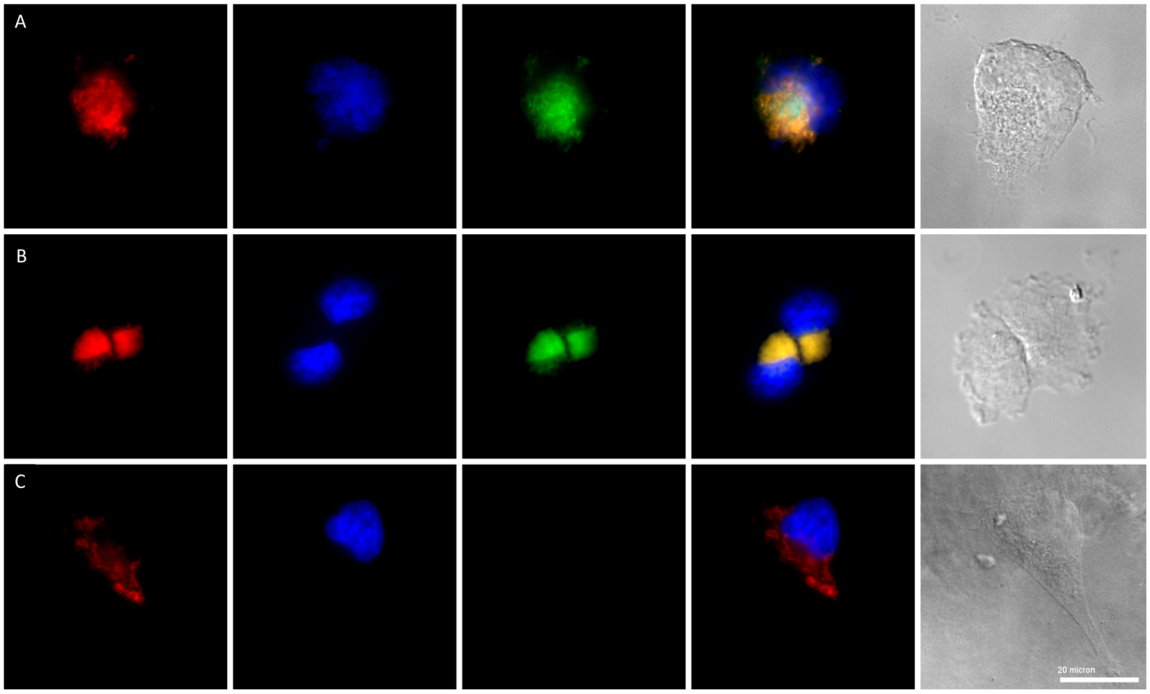


Figure 2. Fluorescence microscopy of MRC-5 cells treated with compound **2a**. Cells were incubated with 5 μM of compound **2a** (green channel) for 30 min (**A**) and 2 h (**B**). The mitochondria stain is represented in the red channel, and the nuclear stain is represented in the blue channel. The negative control is displayed in row (**C**). Scale bar: 20 μm.

MRC-5 cells were incubated with 5 μM of **2a** for 30 min (Figure 2A) and 2 h (Figure 2B), and in both time points, we could detect the compound inside the cells (green channel). Moreover, the mitochondria were stained with a commercial probe (MitoTracker deep red, red channel), and as we can observe in the merged images, there is an overlap between the green and red channel fluorescence, resulting in a yellow signal. Pearson's correlation coefficient (PCC) was used to quantify the extent of overlap between the two channels. PCC values of 0.83 $\pm$ 0.05 and 0.95 $\pm$ 0.06 were found for the overlap of compound **2a** and the MitoTracker after 30 min and 2 h of incubation, respectively. These results corroborate

the strong correlation between these two probes, suggesting that compound **2a** may be accumulating in the mitochondria.

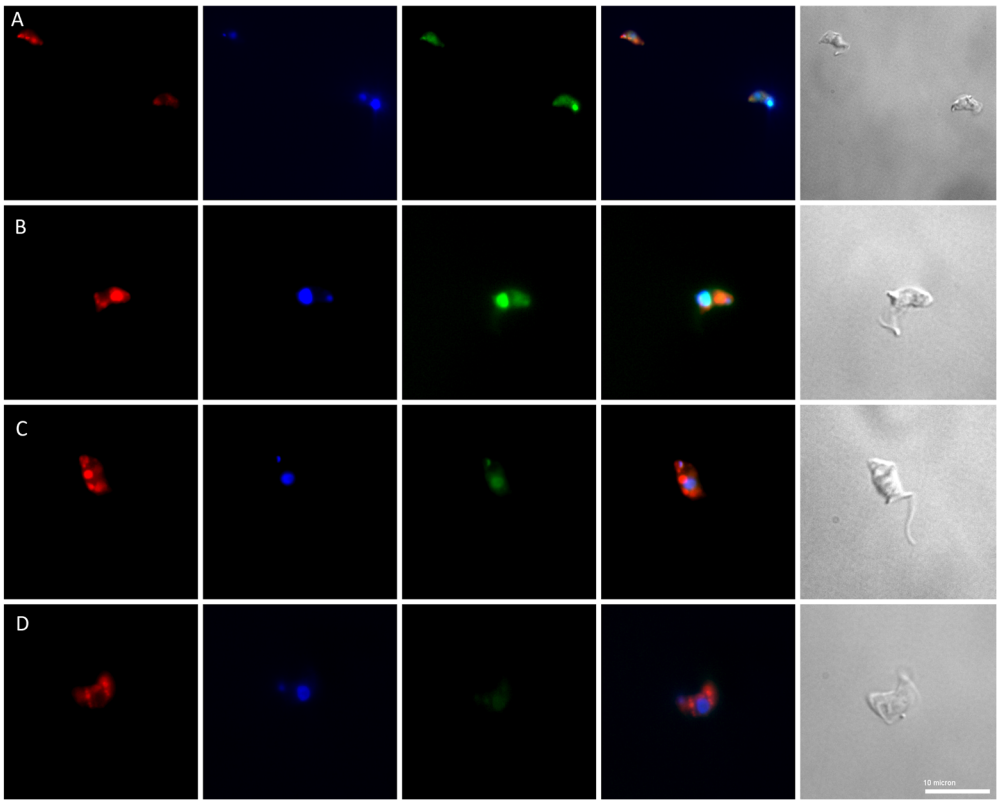


Figure 3. Fluorescence microscopy of parasites *T. brucei* treated with compound **2a**. Parasites were incubated with 5 μM of compound **2a** (green channel) for 30 min (**A**); 1 h (**B**); and 2 h (**C**). The mitochondria stain is represented in the red channel, and the nuclear stain is represented in the blue channel. The negative control is displayed in row (**D**). Scale bar: 10 μm.

T. brucei parasites were also incubated with 5 μM of **2a** for 30 min (Figure 3A), 1 h (Figure 3B) and 2 h (Figure 3C), and contrary to what was observed in MRC-5 cells, the compound seems to accumulate in the nucleus over time. At 30 min, it exhibits both nuclear and cytosolic localization; however, as the incubation time increases to 1 h and 2 h, the BIM derivative (green channel) appears to overlap with the nucleus dye (blue channel). The PCC values for the overlap of compound **2a** with the nuclear dye after 30 min, 1 h and 2 h of incubation were 0.66 ± 0.19, 0.82 ± 0.08, 0.85 ± 0.08, respectively, which supports the greater accumulation of **2a** within the parasite's nucleus as incubation time progresses.

3. Experimental Section

3.1. General

NMR spectra were obtained on a Bruker Avance III 400 at an operating frequency of 400 MHz for ^{1}H and 100.6 MHz for ^{13}C, using the solvent peak as an internal reference (δ relative to TMS). Peak assignments were supported by spin decoupling-double resonance and bidimensional heteronuclear techniques. High resolution mass spectra (HRMS) were obtained on an ESI/quadrupole mass spectrometer (WATERS, ACQUITY H CLASS). All reagents were purchased from Sigma-Aldrich, Acros and Fluka and used as received. Thin-layer chromatography (TLC) was carried out on 0.25 mm thick precoated silica plates (Merck Fertigplatten Kieselgel $60F_{254}$), and spots were visualized under ultraviolet (UV) light. Mps were determined on a Gallenkamp apparatus. Infrared spectra were recorded on a BOMEM MB 104 spectrophotometer. Fluorescence spectra were collected using a FluoroMax-4 spectrofluorometer. UV-visible absorption spectra (200–700 nm) were

obtained using a Shimadzu UV/2501PC spectrophotometer. Fluorescence quantum yields were measured using 9,10-diphenylanthracene (DPA) in ethanol as standard (ϕ_F = 0.95) [43]. The synthesis of BIM derivative **2a** has been reported previously [39,40].

3.2. Synthesis of Bis(indolyl)methanes Derivatives **2a–c**

$KHSO_4$ (0.56 mmol) was added to a mixture of indole (1.15 mmol) and the aldehydes **1a–c** (0.57 mmol) in dry methanol (3 mL), and the reaction was stirred at room temperature for 7 h [38]. Then, water (3 mL) was added to quench the reaction, and the aqueous phase was extracted with dichloromethane (3 × 20 mL). The organic phase was dried with anhydrous $MgSO_4$, and the crude compounds **2a–c** were purified by recrystallization from dichloromethane.

3.2.1. *Bis*(indolyl)methane **2a** [39,40]

Violet solid (48%); mp: 144.4–145.0 °C. ^{1}H NMR (DMSO-d_6) δ = 5.78 (s, 1H, CH) 6.84–6.87 (m, 2H, H2 and H5), 6.91–6.99 (m, 5H, H2′, H6′, H2″, H4″ and H6″), 7.02 (dt, 1H, J = 8.0 and 0.8 Hz, H6), 7.22 (t, 1H, J = 8.0 Hz, H3″ and H5″), 7.24 (d, 2H, J = 7.6 Hz, H3′ and H5′), 7.31 (d, 1H, J = 8.4 Hz, H4), 7.34 (d, 1H, J = 8.4 Hz, H7), 10.80 (s, 2H, 2 × NH). ^{13}C NMR (DMSO-d_6) δ = 39.0 (CH), 118.2 (C5 and C3), 119.1 (C4), 120.9 (C6), 122.5 (C2′ and C6′), 123.3 (C2″ and C6″), 123.5 (C2), 123.9 (C4″), 126.6 (C3a), 129.3 (C3′ and C5′), 129.4 (C3″ and C5″), 136.5 (C7a), 140.0 (C4′), 144.8 (C1′), 147.4 (C1″). IR (Nujol) ν = 3584, 3557, 3419, 3137, 2672, 2361, 2341, 1934, 1744, 1712, 1587, 1339, 1275, 1216, 1172, 1124, 1090, 1032, 1011, 935, 890, 741, 696 cm^{-1}.

3.2.2. *Bis*(indolyl)methane **2b**

Brown solid (80%); mp: 204.8–205.4 °C. ^{1}H NMR (DMSO-d_6) δ = 2.95 (s, 6H, 2 × CH_3) 6.57 (s, 1H, CH), 6.73 (d, 1H, J = 2.4 Hz, H2), 6.84 (dt, 1H, J = 8.0 and 0.8 Hz, H5), 7.02 (dt, 1H, J = 8.0 and 0.8 Hz, H6), 7.21 (d, 2H, J = 7.2 Hz, H2′ and H3′), 7.26 (d, 1H, J = 8.0 Hz, H4), 7.34 (d, 1H, J = 8.4 Hz, H7), 7.47 (t, 1H, J = 8.2 Hz, H7′), 7.60 (t, 1H, J = 8.2 Hz, H6′), 8.22 (d, 1H, J = 8.4 Hz, H5′), 8.29 (d, 1H, J = 8.4 Hz, H8′), 10.79 (s, 2H, 2 × NH). ^{13}C NMR (DMSO-d_6) δ = 35.2 (CH), 45.5 (2 × CH3), 111.5 (C7), 117.6 (C5), 118.3 (C5), 119.0 (C4), 120.9 (C6), 123.3 (C5′), 124.3 (C2), 124.8 (C8′), 125.4 (C2′, C3′ and C6′) 126.0 (C7′), 126.6 (C3a), 127.4 (C4a′), 132.3 (C8a′), 136.6 (C7a). The signals of C1′ and C4′ are not visible in the ^{13}C NMR. IR (Nujol) ν = 3583, 3223, 3188, 2676, 2360, 2336, 1622, 1602, 1231, 1216, 107, 1054, 1009, 933, 891, 872, 853, 810, 797, 782, 748 cm^{-1}. HRMS (ESI) m/z: $[M + H]^+$ calcd for $C_{29}H_{26}N_3$ 416.2127, found 416.2126.

3.2.3. *Bis*(indolyl)methane **2c**

Green solid (37%); mp: 207.8–208.4 °C. ^{1}H NMR (DMSO-d_6) δ = 6.19 (s, 1H, CH), 6.85 (dt, 1H, J = 8 and 1.2 Hz, H5), 7.01 (dd, 1H, J = 8.0 and 1.2 Hz, H6), 7.04 (d, 1H, J = 2.0 Hz, H2), 7.06 (dd, 1H, J = 7.6 and 1.6 Hz, H4), 7.29–7.36 (m, 4H, H7, H5′, H6′ and H7′), 7.56 (d, 1H, J = 8.8 Hz, H3′), 10.89 (s, 2H, 2 × NH). The signal of OH is not visible in the ^{1}H NMR. IR (Nujol) ν = 3184, 1634, 1599, 1537, 1378, 1091, 1040, 779, 744 cm^{-1}. HRMS (ESI) m/z: $[M + H]^+$ calcd for $C_{26}H_{20}N_3O$ 390.1606, found 390.1593.

3.3. Biological Activity

3.3.1. Parasite and Cell Culturing

T. brucei (Lister 427, antigenic type MiTat 1.2, clone 221a, bloodstream forms, "single marker" S427 (S16)) [44] were cultured at 37 °C, 5% CO_2 in HMI-9 medium supplemented with 10% heat-inactivated fetal bovine serum (hiFBS, Invitrogen), as previously described [45].

L. major (MHOM/IL/80/Friedlin) promastigotes were cultured at 28 °C, 5% CO_2 in modified RPMI-1640 medium (Invitrogen, Carlsbad, CA, USA) supplemented with 10% hiFBS [45]. Parasites were maintained in culture in their experimental growth phase (below 2 million parasites per mL for *T. brucei* and 10 million parasites per mL for *L. major*).

MRC-5 cell line (human lung fibroblast) was grown in monolayer at 37 °C, 5% CO_2 in DMEM medium (1 g/L glucose) supplemented with 10% hiFBS, 100 U/mL penicillin, 100 mg/mL streptomycin and 2 mM L-glutamine [46].

HeLa (human cervical carcinoma) and HT-29 (human colorectal adenocarcinoma) cell lines were maintained at 37 °C, 5% CO_2 in high glucose DMEM (4.5 g/L glucose) supplemented with 10% hiFBS, 100 U/mL penicillin, 100 mg/mL streptomycin, 2 mM L-glutamine and non-essential amino acids (1X). Cells were plated and passaged according to ATCC recommendations and were used for the experiments while in the exponential growth phase.

3.3.2. Anti-Parasitic Activity

The trypanocidal activity of the compounds was assessed using the alamarBlue® assay (ThermoFisher Scientific, Waltham, MA, USA) [46,47]. The stock solutions of the compounds were prepared in DMSO, and the final DMSO percentage in each well was adjusted to be less than 1%. A total of 2×10^4 parasites per mL were incubated at 37 °C, 5% CO_2 in 96-well plates (50 µL/well) alone or in the presence of an increasing concentration of compounds for 72 h. A total of 20 µL of resazurin solution (110 ng/mL) was then added to each well, and the parasites were incubated for 4 h at 37 °C. Finally, cells were lysed with 50 µL per well of SDS 3%. The plate was incubated at 37 °C for an extra hour; then, the fluorescence intensity was measured with an Infinite F200 plate reader (Tecan Austria, GmbH, Grödig, Austria), exciting at 550 nm and recording the emission at 590 nm. The results are expressed as the concentration of the compound that reduces cell growth by 50% versus untreated control cells (IC_{50}). Data are presented as the average of at least three independent measurements all conducted in triplicate.

The leishmanicidal activity of the compounds was determined using MTT-based assay (Sigma-Aldrich, St. Louis, MO, USA) [48]. The stock solutions of the compounds were prepared in DMSO, and the final DMSO percentage in each well was adjusted to be less than 1%. A total of 4×10^6 parasites per mL were incubated at 28 °C in 96-well plates (50 µL/well) alone or in the presence of an increasing concentration of compounds DMSO for 72 h. A total of 10 µL of MTT (5 mg/mL) was added to each well, and parasites were incubated for 4 h at 28 °C. Finally, cells were lysed with 50 µL/well of 20% SDS. The plate was incubated at 37 °C for an extra hour; then, the absorbance was measured with the Infinite F200 plate reader (TECAN Austria, GmbH, Grödig, Austria) at a wavelength of 540 nm. The IC_{50} was calculated as described above. Data are presented as the average of at least three independent measurements all conducted in triplicate.

3.4. Cytotoxicity

Cytotoxicity was measured in MRC-5, HeLa and HT-29 cell lines using alamarBlue® assay (ThermoFisher Scientific) [46,47]. The stock solutions of the compounds were prepared in DMSO, and the final DMSO percentage in each well was adjusted to be less than 1%. A total of 5×10^3 cells per mL (MRC-5, HeLa or HT-29 cells) were seeded in 96-well plates (100 µL/well) with 24 h of incubation time before compound addition at 37 °C, 5% CO_2. Then, the compounds were added at increasing concentrations (from 0 to 100 µM), and the plates were incubated for 72 h. A total of 20 µL of resazurin solution (110 ng/mL) was added to each well, and cells were incubated for 4 h. Then, cells were lysed with 50 µL/well of 3% SDS. The plate was incubated at 37 °C for an extra hour; then, the fluorescence intensity was measured with the Infinite F200 plate reader (TECAN Austria, GmbH), exciting at 550 nm and recording the emission at 590 nm. The results are expressed as the concentration of compound that reduces cell growth by 50% versus untreated control cells (IC_{50}). Data are presented as the average of at least three independent measurements all conducted in triplicate.

3.5. In Silico Evaluation of the Physicochemical and Pharmacokinetic Properties

The physicochemical and pharmacokinetic properties of the compounds were predicted using ADMET (absorption, distribution, metabolism, excretion and toxicity) profiles available in the ADMET lab 2.0 online server https://admetmesh.scbdd.com/ (accessed on 10 September 2023) [42].

3.6. Fluorescence Microscopy

MRC-5 cells (2×10^4/mL) were incubated with 5 μM of compound **2a** in 0.5 mL of their respective medium for 30 min and 1 h at 37 °C and 100% humidity. Mitochondrial and nuclear staining was performed with MitoTracker deep red (200 nM) and green nuclear dye (2 drops/mL), respectively, for 30 min. Cells were washed five times with room temperature PBS and fixed with 2% paraformaldehyde for 20 min and washed two extra times with PBS. Then, the cover slides were immerged in water, and ethanol immersion of the cover slide was also necessary prior to sample processing for microscopy.

T. Brucei parasites (2×10^7/mL) were incubated with 5 μM of compound **2a** in 0.5 mL of their respective medium for 30 min, 1 h and 2 h at 37 °C and 100% humidity. Mitochondrial and nuclear staining was performed with MitoTracker deep red (200 nM) and green nuclear dye (2 drops/mL), respectively, for 30 min. Parasites were washed five times with cold PBS and fixed with paraformaldehyde 4% for 20 min, washed two extra times with cold PBS and processed by microscope observation.

Images were acquired using a widefield Olympus ix81 microscope. Excitation was carried out with the 490 nm, 385 nm and 633 nm filters for green nuclear dye, compound **2a** and MitoTracker, respectively. Emission was detected at 512–548 nm for green nuclear dye, 420–450 nm for compound **2a** and 666–724 nm for MitoTracker. The images were processed and analyzed with Fiji software 64 bits version for windows (https://fiji.sc/, accessed on 10 September 2023).

4. Conclusions

In this work, we reported the synthesis of *bis*(indolyl)methane derivatives functionalized with triphenylamine, *N*,*N*-dimethyl-1-naphthylamine and 8-hydroxylquinolyl groups. The influence of the hetero(aromatic) moieties on their biological activity in the pathogenic parasites *T. brucei* and *L. major*, and as well as in the cancer cell lines HT-29 and HeLa, was investigated.

The antiparasitic activity studies revealed that the BIM substituted with triphenylamine (**2a**) displayed the best toxicity and selectivity of the series against *Trypanosoma brucei* and *Leishmania major* (with an IC_{50} of 3.21 and 3.30 μM, respectively, and ≈10-fold selectivity over healthy cell line MRC-5). Compound **2a** also showed a higher inhibitory effect against HT-29 cells than against HeLa cells, with an IC_{50} of 3.93 μM and selectivity index of 8.57. Its antiproliferative activity was found to be remarkably more active than its unsubstituted analogue, 3,3-diindolylmethane (IC_{50} > 100 μM against HT-29 cell line). Moreover, the internalization studies using fluorescence microscopy suggested that compound **2a** localizes in the mitochondria in MRC-5 cells and in the nucleus in *T. brucei* parasites. In conclusion, the *bis*(indolyl)methane derivative **2a** was demonstrated to be a potential candidate as a trypanocidal and leishmanicidal agent and as a chemotherapy drug against colon cancer.

Supplementary Materials: The following supporting information can be downloaded at https://www.mdpi.com/article/10.3390/molecules28237728/s1; Figure S1: ^{1}H NMR spectra of BIM **2a** in DMSO-d_6; Figure S2: ^{13}C NMR spectra of BIM **2a** in DMSO-d_6; Figure S3: ^{1}H NMR spectra of BIM **2b** in DMSO-d_6; Figure S4: ^{13}C NMR spectra of BIM **2b** in DMSO-d_6; Figure S5: ^{1}H NMR spectra of BIM **2c** in DMSO-d_6; Figure S6: normalized UV-visible absorption and emission spectra of BIM **2a** in ACN solution; Figure S7: dose-response curve of BIM **2a**–**c** in *T. brucei* parasites; Figure S8: dose-response curve of BIM **2a**–**c** in *L. major* parasites; Figure S9: dose-response curve of BIM **2a**–**c** in HeLa cells;

Figure S10: dose-response curve of BIM **2a–c** in HT-29 cells; Figure S11: cell viability of *T. brucei*, *L. major*, HeLa and HT-29 cells treated with DMSO 1%.

Author Contributions: Conceptualization, R.C.R.G., P.P., J.C.M. and M.M.M.R.; methodology, R.C.R.G., P.P., J.C.M. and M.M.M.R.; validation, S.P.G.C., P.P. and M.M.M.R.; formal analysis, R.C.R.G., P.P., J.C.M. and M.M.M.R.; investigation, R.C.R.G. and P.P.; resources, S.P.G.C., J.C.M. and M.M.M.R.; writing—original draft preparation, R.C.R.G.; writing—review and editing, R.C.R.G., P.P., S.P.G.C., J.C.M. and M.M.M.R.; supervision, S.P.G.C., J.C.M. and M.M.M.R.; project administration, S.P.G.C. and M.M.M.R.; funding acquisition, S.P.G.C. and M.M.M.R. All authors have read and agreed to the published version of the manuscript.

Funding: This research was funded by Fundação para a Ciência e Tecnologia (FCT) and FEDER (European Fund for Regional Development)-COMPETE-QRENEU through the Chemistry Research Centre of the University of Minho CQ-UM (UID/QUI/00686/2020), project PTDC/QUI-OUT/3143/2021 and a PhD grant to R.C.R. Gonçalves (SFRH/BD/05278/2020). The NMR spectrometer Bruker Avance III 400 is part of the National NMR Network and was purchased within the framework of the National Program for Scientific Re-equipment, contract REDE/1517/RMN/2005 with funds from POCI 2010 (FEDER) and FCT.

Institutional Review Board Statement: Not applicable.

Informed Consent Statement: Not applicable.

Data Availability Statement: Data are contained within the article and Supplementary Materials.

Acknowledgments: The authors thank Efres Belmonte Reche for his help regarding this topic. For the graphical abstract image: the trypanosoma icon by Servier https://smart.servier.com/ (accessed on 2 November 2023) is licensed under CC-BY 3.0 Unported https://creativecommons.org/licenses/by/3.0/ (accessed on 2 November 2023); cell-HeLa icon by DBCLS https://togotv.dbcls.jp/en/pics.html (accessed on 2 November 2023) is licensed under CC-BY 4.0 Unported https://creativecommons.org/licenses/by/4.0/ (accessed on 2 November 2023).

Conflicts of Interest: The authors declare no conflict of interest.

References

1. Moafi, M.; Rezvan, H.; Sherkat, R.; Taleban, R. Leishmania Vaccines Entered in Clinical Trials: A Review of Literature. *Int. J. Prev. Med.* **2019**, *10*, 95. [CrossRef] [PubMed]
2. Malvolti, S.; Malhame, M.; Mantel, C.F.; Le Rutte, E.A.; Kaye, P.M. Human Leishmaniasis Vaccines: Use Cases, Target Population and Potential Global Demand. *PLoS Negl. Trop. Dis.* **2021**, *15*, e0009742. [CrossRef] [PubMed]
3. La Greca, F.; Magez, S. Vaccination against Trypanosomiasis: Can It Be Done or Is the Trypanosome Truly the Ultimate Immune Destroyer and Escape Artist? *Hum. Vaccin.* **2011**, *7*, 1225–1233. [CrossRef]
4. Autheman, D.; Crosnier, C.; Clare, S.; Goulding, D.A.; Brandt, C.; Harcourt, K.; Tolley, C.; Galaway, F.; Khushu, M.; Ong, H.; et al. An Invariant Trypanosoma Vivax Vaccine Antigen Induces Protective Immunity. *Nature* **2021**, *595*, 96–100. [CrossRef] [PubMed]
5. Bernhard, S.; Kaiser, M.; Burri, C.; Mäser, P. Fexinidazole for Human African Trypanosomiasis, the Fruit of a Successful Public-Private Partnership. *Diseases* **2022**, *10*, 90. [CrossRef]
6. Chavan, K.A.; Shukla, M.; Chauhan, A.N.S.; Maji, S.; Mali, G.; Bhattacharyya, S.; Erande, R.D. Effective Synthesis and Biological Evaluation of Natural and Designed *Bis*(Indolyl)Methanes via Taurine-Catalyzed Green Approach. *ACS Omega* **2022**, *7*, 10438–10446. [CrossRef]
7. Jella, R.R.; Nagarajan, R. Synthesis of Indole Alkaloids Arsindoline A, Arsindoline B and Their Analogues in Low Melting Mixture. *Tetrahedron* **2013**, *69*, 10249–10253. [CrossRef]
8. Praveen, P.; Parameswaran, P.; Majik, M. *Bis*(Indolyl)Methane Alkaloids: Isolation, Bioactivity, and Syntheses. *Synthesis* **2015**, *47*, 1827–1837. [CrossRef]
9. Marrelli, M.; Cachet, X.; Conforti, F.; Sirianni, R.; Chimento, A.; Pezzi, V.; Michel, S.; Statti, G.A.; Menichini, F. Synthesis of a New *Bis*(Indolyl)Methane That Inhibits Growth and Induces Apoptosis in Human Prostate Cancer Cells. *Nat. Prod. Res.* **2013**, *27*, 2039–2045. [CrossRef]
10. Tian, X.; Liu, K.; Zu, X.; Ma, F.; Li, Z.; Lee, M.; Chen, H.; Li, Y.; Zhao, Y.; Liu, F.; et al. 3,3′-Diindolylmethane Inhibits Patient-Derived Xenograft Colon Tumor Growth by Targeting COX1/2 and ERK1/2. *Cancer Lett.* **2019**, *448*, 20–30. [CrossRef]
11. Lee, J. 3,3′-Diindolylmethane Inhibits TNF-α- and TGF-β-Induced Epithelial–Mesenchymal Transition in Breast Cancer Cells. *Nutr. Cancer* **2019**, *71*, 992–1006. [CrossRef] [PubMed]
12. Bahuguna, A.; Singh, A.; Kumar, P.; Dhasmana, D.; Krishnan, V.; Garg, N. Bisindolemethane Derivatives as Highly Potent Anticancer Agents: Synthesis, Medicinal Activity Evaluation, Cell-Based Compound Discovery, and Computational Target Predictions. *Comput. Biol. Med.* **2020**, *116*, 103574. [CrossRef] [PubMed]

13. Imran, S.; Taha, M.; Ismail, N.; Khan, K.; Naz, F.; Hussain, M.; Tauseef, S. Synthesis of Novel Bisindolylmethane Schiff Bases and Their Antibacterial Activity. *Molecules* **2014**, *19*, 11722–11740. [CrossRef]
14. Roy, S.; Gajbhiye, R.; Mandal, M.; Pal, C.; Meyyapan, A.; Mukherjee, J.; Jaisankar, P. Synthesis and Antibacterial Evaluation of 3,3′-Diindolylmethane Derivatives. *Med. Chem. Res.* **2014**, *23*, 1371–1377. [CrossRef]
15. Fan, S.; Meng, Q.; Saha, T.; Sarkar, F.H.; Rosen, E.M. Low Concentrations of Diindolylmethane, a Metabolite of Indole-3-Carbinol, Protect against Oxidative Stress in a BRCA1-Dependent Manner. *Cancer Res.* **2009**, *69*, 6083–6091. [CrossRef]
16. Benabadji, S.H.; Wen, R.; Zheng, J.; Dong, X.; Yuan, S. Anticarcinogenic and Antioxidant Activity of Diindolylmethane Derivatives. *Acta Pharmacol. Sin.* **2004**, *25*, 666–671.
17. De Miranda, B.R.; Miller, J.A.; Hansen, R.J.; Lunghofer, P.J.; Safe, S.; Gustafson, D.L.; Colagiovanni, D.; Tjalkens, R.B. Neuroprotective Efficacy and Pharmacokinetic Behavior of Novel Anti-Inflammatory *Para* -Phenyl Substituted Diindolylmethanes in a Mouse Model of Parkinson's Disease. *J. Pharmacol. Exp. Ther.* **2013**, *345*, 125–138. [CrossRef]
18. Sujatha, K.; Perumal, P.T.; Muralidharan, D.; Rajendran, M. Synthesis, Analgesic and Antiinflammatory Activities of Bis(Indolyl)Methanes. *ChemInform* **2009**, *40*, 267–272. [CrossRef]
19. Sivaprasad, G.; Perumal, P.T.; Prabavathy, V.R.; Mathivanan, N. Synthesis and Anti-Microbial Activity of Pyrazolylbisindoles—Promising Anti-Fungal Compounds. *Bioorganic Med. Chem. Lett.* **2006**, *16*, 6302–6305. [CrossRef]
20. Kang, J.; Gao, Y.; Zhang, M.; Ding, X.; Wang, Z.; Ma, D.; Wang, Q. Streptindole and Its Derivatives as Novel Antiviral and Anti-Phytopathogenic Fungus Agents. *J. Agric. Food Chem.* **2020**, *68*, 7839–7849. [CrossRef]
21. Imran, S.; Taha, M.; Ismail, N. A Review of Bisindolylmethane as an Important Scaffold for Drug Discovery. *Curr. Med. Chem.* **2015**, *22*, 4412–4433. [CrossRef] [PubMed]
22. Koli, P.; Reena; Indurthi, H.K.; Sharma, D.K. Anticancer Activity of 3,3′-Diindolylmethane and the Molecular Mechanism Involved in Various Cancer Cell Lines. *ChemistrySelect* **2020**, *5*, 11540–11548. [CrossRef]
23. Biersack, B. 3,3′-Diindolylmethane and Its Derivatives: Nature-Inspired Strategies Tackling Drug Resistant Tumors by Regulation of Signal Transduction, Transcription Factors and microRNAs. *Cancer Drug Resist.* **2020**, *3*, 867–878. [CrossRef]
24. Choi, H.J.; Lim, D.Y.; Park, J.H.Y. Induction of G1 and G2/M Cell Cycle Arrests by the Dietary Compound 3,3′-Diindolylmethane in HT-29 Human Colon Cancer Cells. *BMC Gastroenterol.* **2009**, *9*, 39. [CrossRef]
25. Kim, S. 3,3′-Diindolylmethane Suppresses Growth of Human Esophageal Squamous Cancer Cells by G1 Cell Cycle Arrest. *Oncol. Rep.* **2012**, *27*, 1669. [CrossRef]
26. Chang, X. 3,3′-Diindolylmethane Inhibits Angiogenesis and the Growth of Transplantable Human Breast Carcinoma in Athymic Mice. *Carcinogenesis* **2005**, *26*, 771–778. [CrossRef] [PubMed]
27. Munakarmi, S.; Shrestha, J.; Shin, H.-B.; Lee, G.-H.; Jeong, Y.-J. 3,3′-Diindolylmethane Suppresses the Growth of Hepatocellular Carcinoma by Regulating Its Invasion, Migration, and ER Stress-Mediated Mitochondrial Apoptosis. *Cells* **2021**, *10*, 1178. [CrossRef] [PubMed]
28. Taha, M.; Uddin, I.; Gollapalli, M.; Almandil, N.B.; Rahim, F.; Farooq, R.K.; Nawaz, M.; Ibrahim, M.; Alqahtani, M.A.; Bamarouf, Y.A.; et al. Synthesis, Anti-Leishmanial and Molecular Docking Study of Bis-Indole Derivatives. *BMC Chem.* **2019**, *13*, 102. [CrossRef] [PubMed]
29. Bharate, S.B.; Bharate, J.B.; Khan, S.I.; Tekwani, B.L.; Jacob, M.R.; Mudududdla, R.; Yadav, R.R.; Singh, B.; Sharma, P.R.; Maity, S.; et al. Discovery of 3,3′-Diindolylmethanes as Potent Antileishmanial Agents. *Eur. J. Med. Chem.* **2013**, *63*, 435–443. [CrossRef]
30. Roy, A.; Ganguly, A.; BoseDasgupta, S.; Das, B.B.; Pal, C.; Jaisankar, P.; Majumder, H.K. Mitochondria-Dependent Reactive Oxygen Species-Mediated Programmed Cell Death Induced by 3,3′-Diindolylmethane through Inhibition of F0F1-ATP Synthase in Unicellular Protozoan Parasite *Leishmania donovani*. *Mol. Pharmacol.* **2008**, *74*, 1292–1307. [CrossRef]
31. Roy, A.; Das, B.B.; Ganguly, A.; Bose Dasgupta, S.; Khalkho, N.V.M.; Pal, C.; Dey, S.; Giri, V.S.; Jaisankar, P.; Dey, S.; et al. An Insight into the Mechanism of Inhibition of Unusual Bi-Subunit Topoisomerase I from *Leishmania Donovani* by 3,3′-Di-Indolylmethane, a Novel DNA Topoisomerase I Poison with a Strong Binding Affinity to the Enzyme. *Biochem. J.* **2008**, *409*, 611–622. [CrossRef]
32. Roy, A.; Chowdhury, S.; Sengupta, S.; Mandal, M.; Jaisankar, P.; D'Annessa, I.; Desideri, A.; Majumder, H.K. Development of Derivatives of 3, 3′-Diindolylmethane as Potent *Leishmania Donovani* Bi-Subunit Topoisomerase IB Poisons. *PLoS ONE* **2011**, *6*, e28493. [CrossRef]
33. Zeligs, M.A. Anti-Parasitic Methods and Compositions Utilizing Diindolylmethane-Related Indoles. US20100055201A1, 19 November 2013.
34. Dorosti, Z.; Yousefi, M.; Sharafi, S.M.; Darani, H.Y. Mutual Action of Anticancer and Antiparasitic Drugs: Are There Any Shared Targets? *Future Oncol.* **2014**, *10*, 2529–2539. [CrossRef] [PubMed]
35. Li, Y.-Q.; Zheng, Z.; Liu, Q.-X.; Lu, X.; Zhou, D.; Zhang, J.; Zheng, H.; Dai, J.-G. Repositioning of Antiparasitic Drugs for Tumor Treatment. *Front. Oncol.* **2021**, *11*, 670804. [CrossRef] [PubMed]
36. Belmonte-Reche, E.; Benassi, A.; Peñalver, P.; Cucchiarini, A.; Guédin, A.; Mergny, J.L.; Rosu, F.; Gabelica, V.; Freccero, M.; Doria, F.; et al. Thiosugar Naphthalene Diimide Conjugates: G-Quadruplex Ligands with Antiparasitic and Anticancer Activity. *Eur. J. Med. Chem.* **2022**, *232*, 114183. [CrossRef] [PubMed]
37. O'Hagan, M.P.; Peñalver, P.; Gibson, R.S.L.; Morales, J.C.; Galan, M.C. Stiff-Stilbene Ligands Target G-Quadruplex DNA and Exhibit Selective Anticancer and Antiparasitic Activity. *Chem. Eur. J.* **2020**, *26*, 6224–6233. [CrossRef]
38. Nagarajan, R.; Perumal, P.T. Potassium Hydrogen Sulfate-Catalyzed Reactions of Indoles: A Mild, Expedient Synthesis of Bis-Indolylmethanes. *Chem. Lett.* **2004**, *33*, 288–289. [CrossRef]

39. Xu, J.; Shang, W.; Zhu, J.; Cheng, Z.; Zhou, N.; Zhu, X. Synthesis and Characterization of Triphenylamine and Bis(Indolyl)Methane Center-Functionalized Polymer via Reversible Addition-Fragmentation Chain Transfer Polymerization. *e-Polymers* **2008**, *8*, 024. [CrossRef]
40. Zarandi, M.; Salimi Beni, A. Synthesis and DFT Calculation on Novel Derivatives of *Bis*-(Indolyl) Methanes. *J. Mol. Struct.* **2016**, *1119*, 404–412. [CrossRef]
41. Ahmad, A.; Dandawate, P.; Schruefer, S.; Padhye, S.; Sarkar, F.H.; Schobert, R.; Biersack, B. Pentafluorophenyl Substitution of Natural Di(Indol-3-yl)Methane Strongly Enhances Growth Inhibition and Apoptosis Induction in Various Cancer Cell Lines. *Chem. Biodivers.* **2019**, *16*, e1900028. [CrossRef]
42. Xiong, G.; Wu, Z.; Yi, J.; Fu, L.; Yang, Z.; Hsieh, C.; Yin, M.; Zeng, X.; Wu, C.; Lu, A.; et al. ADMETlab 2.0: An Integrated Online Platform for Accurate and Comprehensive Predictions of ADMET Properties. *Nucleic Acids Res.* **2021**, *49*, W5–W14. [CrossRef] [PubMed]
43. Montalti, M.; Credi, A.; Prodi, L.; Gandolfi, M.T. *Handbook of Photochemistry*, 3rd ed.; CRC Press: Boca Raton, FL, USA, 2006; ISBN 978-0-429-11538-7.
44. Wirtz, E.; Leal, S.; Ochatt, C.; Cross, G.A.M. A Tightly Regulated Inducible Expression System for Conditional Gene Knock-Outs and Dominant-Negative Genetics in *Trypanosoma brucei*. *Mol. Biochem. Parasitol.* **1999**, *99*, 89–101. [CrossRef] [PubMed]
45. Cabello-Donayre, M.; Malagarie-Cazenave, S.; Campos-Salinas, J.; Gálvez, F.J.; Rodríguez-Martínez, A.; Pineda-Molina, E.; Orrego, L.M.; Martínez-García, M.; Sánchez-Cañete, M.P.; Estévez, A.M.; et al. Trypanosomatid Parasites Rescue Heme from Endocytosed Hemoglobin through Lysosomal HRG Transporters: Trypanosomatid HRG Proteins Rescue Heme from Hb. *Mol. Microbiol.* **2016**, *101*, 895–908. [CrossRef]
46. Belmonte-Reche, E.; Martínez-García, M.; Guédin, A.; Zuffo, M.; Arévalo-Ruiz, M.; Doria, F.; Campos-Salinas, J.; Maynadier, M.; López-Rubio, J.J.; Freccero, M.; et al. G-Quadruplex Identification in the Genome of Protozoan Parasites Points to Naphthalene Diimide Ligands as New Antiparasitic Agents. *J. Med. Chem.* **2018**, *61*, 1231–1240. [CrossRef] [PubMed]
47. Larson, E.M.; Doughman, D.J.; Gregerson, D.S.; Obritsch, W.F. A New, Simple, Nonradioactive, Nontoxic in Vitro Assay to Monitor Corneal Endothelial Cell Viability. *Invest. Ophtalmol. Vis. Sci.* **1997**, *38*, 1929–1933.
48. Pérez-Victoria, J.M.; Bavchvarov, B.I.; Torrecillas, I.R.; Martínez-García, M.; López-Martín, C.; Campillo, M.; Castanys, S.; Gamarro, F. Sitamaquine Overcomes ABC-Mediated Resistance to Miltefosine and Antimony in *Leishmania*. *Antimicrob. Agents Chemother.* **2011**, *55*, 3838–3844. [CrossRef] [PubMed]

Disclaimer/Publisher's Note: The statements, opinions and data contained in all publications are solely those of the individual author(s) and contributor(s) and not of MDPI and/or the editor(s). MDPI and/or the editor(s) disclaim responsibility for any injury to people or property resulting from any ideas, methods, instructions or products referred to in the content.